Optical Fiber Technology 71 (2022) 102919

Contents lists available at ScienceDirect

Optical Fiber Technology

journal homepage: www.elsevier.com/locate/yofte

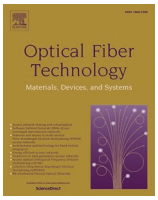

Regular Articles

Understanding the impact of cladding modes in multi-mode hollow-core anti-resonant fibres

William Shere *, Gregory T. Jasion, Eric Numkam Fokoua, Francesco Poletti

Optoelectronics Research Centre, University of Southampton, Southampton SO17 1BJ, United Kingdom

ARTICLE INFO

Keywords:
Hollow-core
Anti-resonant fibre
Multi-mode guidance
Microstructured-optical-fibre
Confinement loss

ABSTRACT

Multi-moded, anti-resonant hollow-core fibre shows great promise for a range of applications from high power laser delivery to novel, non-linear experiments. Anti-resonant fibers typically guide multiple transverse modes due to their large core size, albeit with often large differential modal loss. Understanding the behaviour of higher order modes in these fibres is of crucial importance if we are to exploit the benefits of hollow-core optical guidance in few- and multi-moded applications, or to design more robustly single mode fibres. In this work we conduct thorough numerical investigations into the origins of confinement loss in tubular anti-resonant fibres and its dependence on the fibre's key structural parameters.

We show that away from the resonances in the glass, leakage loss can be interpreted as originating from resonant out-coupling between the core modes of interest and the lossy modes of the cladding tubes, and is highest when these are phase-matched. Using this insight, we show that the loss can be estimated *a posteriori* from knowledge of the fields of the core-guided and cladding tube modes and their propagation constants. Such a quantitative estimate is satisfactory by considering only the three lowest mode groups of the cladding tube. This deeper understanding paves the way to a more informed approach to designing few and multi-moded hollow-core fibers for various applications.

1. Introduction

Hollow-core fibres allow the confinement and guidance of light over considerable distances and at high power levels through air, gas or liquid media [1,2]. Anti-resonant fibres (ARFs), and in particular the Nested Anti-Resonant Nodeless Fibres (NANF) geometry have witnessed phenomenal progress over the past few years. Recent fabricated fibres have achieved comparable loss to solid-core fibres in the C and L telecom bands and much lower loss than the fundamental loss limits of solid-core fibre at wavelengths below 1 μm and in the mid infrared region above 2 μm [3–5]. Furthermore, numerical simulations predict that still lower loss is achievable in such hollow-core fibres.

The guidance mechanism in ARFs is based on coherent reflections from the thin membranes, with recent examples favouring a non-contacting tube cladding that can achieve both lower losses and broader bandwidths than other designs. Low-loss operation often dictates core sizes that are at least 20 times the operating wavelength, resulting in fibres that inherently support multiple transverse modes. One important and intrinsic contribution to loss in ARFs is leakage or confinement loss, which increases with the mode order [6]. This built-in differential loss has been exploited and enhanced to achieve effective single-mode operation for applications such as telecoms where inter-modal interference must be minimized [7]. However, many scenarios and applications such as high-power few-moded laser delivery, short-haul VCSEL-based communications, non-linear optics etc, where multi-mode operation is highly desirable or necessary could benefit from the low-loss, large-bandwidths, high-power capabilities or indeed the low non-linearity that hollow-core fibres are capable of [8,1,2,9]. To develop high performance multi-mode hollow-core optical fibres to be deployed in such applications, we must seek to understand and minimize the differential loss between modes.

An all-encompassing model for predicting the loss of the fundamental and higher modes of ARFs remains beyond reach as solving Maxwell's equations even for the simplest such structures must make use of numerical tools. Higher-order modes have received little attention as the research focus has firmly been on effectively single moded fibres. Indeed, simple design rules have been developed [7,10] to make the fibres effectively single mode, whereas few works have considered

* Corresponding author.
E-mail address: w.shere@soton.ac.uk (W. Shere).

https://doi.org/10.1016/j.yofte.2022.102919
Received 6 December 2021; Received in revised form 11 February 2022; Accepted 26 April 2022
Available online 8 May 2022

multimoded operation in these fibers [11,12].

In this paper, we explore pathways to designing multi-mode hollow-core fibres in which the differential loss between the fundamental and a desired number of higher order modes is kept within a given constraint. Limiting our exploration to the mechanisms of leakage loss, we start by presenting an intuitive understanding of this mechanism in ARFs. We show that away from the glass resonances, leakage results from the coupling between the core-guided and the radiative modes supported in the rest of the structure. When core and lossy cladding modes are phase-matched, the result is prohibitively high leakage loss for the core mode. Reducing the loss therefore requires a large separation in effective index between core and cladding modes as well as minimum spatial overlap between their mode fields. We present results describing this relationship, demonstrate which cladding modes are most significant for different geometries and discuss how to leverage these ideas for the design of few-moded hollow core fibres.

2. Mode structure and mode coupling in anti-resonant fibres

In ARFs, a carefully designed cladding, often consisting of an arrangement of capillaries around a central core, allows light to be confined and guided in said central region. Fig. 1(a) shows an example of hollow-core anti-resonant fibre geometries in which the cladding tubes are not contacting (nodeless). Here, we consider that partitions created by the arrangement of the cladding tubes form a collection of waveguides capable of supporting their own modes when isolated. These regions are the central hollow-core, the dielectric tubes, the hollow air-filled regions enclosed by the tubes, the spaces between the tubes, and the surrounding silica jacket.

Seen this way, the modes supported by the fibre are effectively supermodes of the complex structure and can be conceived as a linear superposition of the modes of the individual constituent waveguides. Fig. 1(c-g) shows contour plots of power distributions of modes confined predominantly in each of these constituent waveguides. We postulate that at wavelengths away from the resonances in the glass membranes, it is the coupling between the core guided modes of interest and these "cladding modes", which themselves suffer substantial attenuation as they can easily couple to radiation modes, which leads to leakage or confinement loss. The modes of the cladding are often far more readily analysed than those of the core. In this case, assuming the loss of these cladding modes is known, coupled-mode analysis can provide an important insight into the loss process of the core modes of interest. Indeed, such an approach was used earlier to explain the high loss suffered by the fundamental mode of hollow-core photonic bandgap fibers in the vicinity of anti-crossing events with lossy surface modes [13,14], and also extensively to interpret the loss in ARFs near the cut off of the modes confined in the glass membranes [15,16]. In [13] it was shown that the additional loss due to coupling with a lossy surface mode would scale approximately as:

$$\alpha \propto \frac{\gamma |\kappa|^2}{(\Delta\beta)^2} \tag{1}$$

where γ is the assumed known loss of the cladding mode, κ the amplitude coupling coefficient between core and cladding mode and $\Delta\beta$ is the difference between their phase constants. Despite being an approximation, (1) shows powerfully that the stronger the spatial overlap between the two mode fields (as captured by the coupling coefficient κ), the

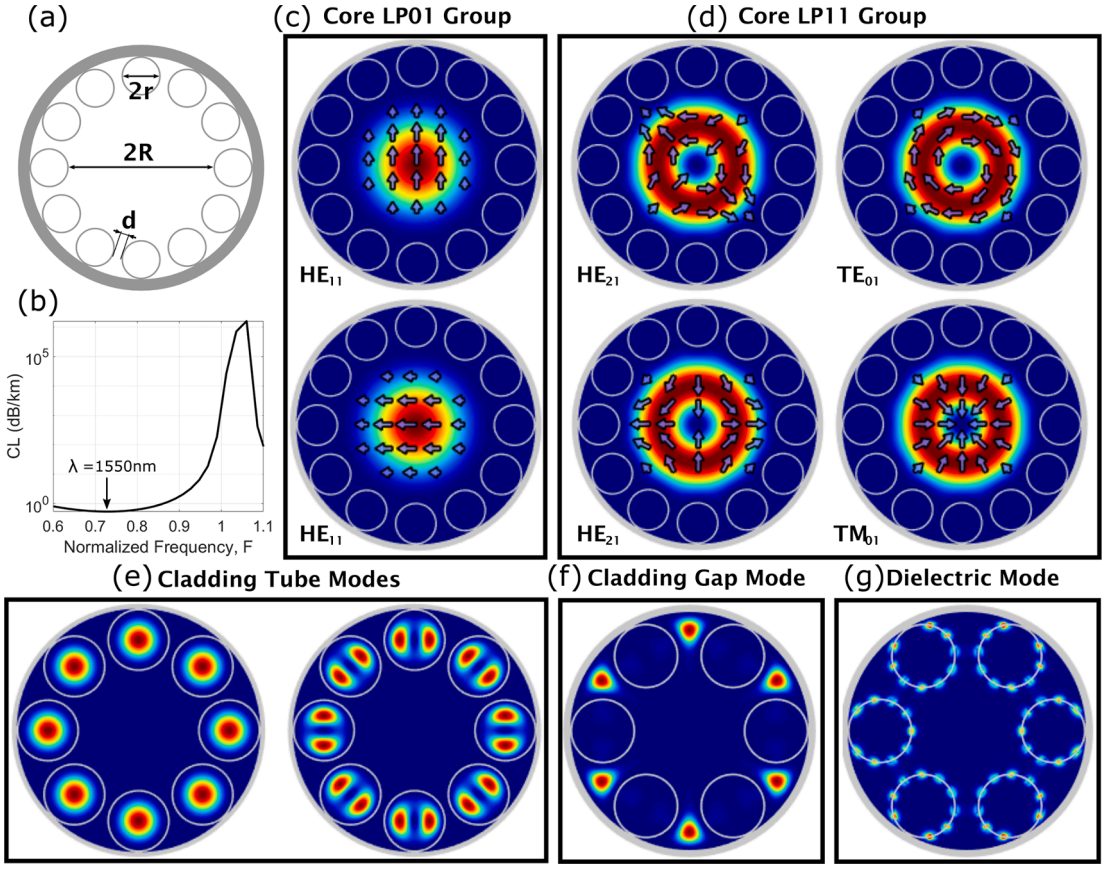

Fig. 1. (a) The geometry of a tubular fibre. (b) Confinement loss spectrum of the fundamental core mode of (a) showing the fundamental anti-resonant window plotted as a function of normalized frequency *F*. Representative examples of (c,d) the core modes and (e,f,g) the cladding modes existent in tubular and NANF ARFs; contour plots describe power flow in the axial direction and arrows denote the transverse electric field. In order to show clearer examples of cladding modes, different geometries have been chosen; these series of modes are present in all tubular fibres.

stronger the loss. Further, and more importantly, the closer the separation between their phase constants (smaller $|\Delta\beta|$), the higher the loss. It is precisely this latter effect that is exploited in designing effectively single mode hollow-core fibers, i.e. by matching the phase constant of the lowest-order HOM to that of the fundamental lossy cladding mode, ensuring that all other HOMs also suffer significantly high loss [7,5]. Interestingly, the Lorentzian shape of (1) has been found to explain very well the loss of core modes in ARFs near the cut-off of the dielectric tube modes where their overlap is not negligible [15,16].

With this understanding, one can therefore postulate that the loss of a given core mode, α_p^{core}, is given by:

$$\alpha_p^{\text{core}} \approx \sum_q \frac{\gamma_k |\kappa_{p,q}|^2}{(\Delta\beta_{p,q})^2} \tag{2}$$

where the summation extends over all the discrete cladding modes and takes the meaning of an integral over the continuum of radiation modes of the silica jacket cladding. Whilst conceptually straightforward, the great difficulty in estimating the loss of the fibre using this expression lies in the fact that the summation extends over a large number of modes, many of which are not easily computed without the use of numerical simulation. This difficulty is greater still if the anti-resonant structure of interest has non-uniformities in tube thicknesses or contacting tubes, because the contact points result in glass nodes which support modes of their own. It is paramount in the design of low-loss structures to avoid such contact points altogether, or alternatively to ensure they are located far away from the core region where the modes of interest are confined (to minimize the coupling coefficient κ) [17–19,10].

The geometry of the fibre determines the modes to which the coupling is strongest and that result in leakage. In particular, for the same number of tubes a design with large gaps will necessarily have smaller capillaries which brings the surrounding silica jacket closer to the core region, thus an increase in direct coupling between the core modes and the continuum of radiation modes supported by the silica jacket. When the gaps are smaller however, the silica jacket is sufficiently far away from the core and a simpler analysis considering only the modes in the hollow regions of the cladding provide adequate insight. We therefore restrict our analysis to such structures with small inter-tube gaps as they have higher potential for low loss operation. In this work we define a small inter-tube gap $d < 4\lambda$ for operational wavelength λ, Fig. 1(a).

Under these conditions, useful simplifications can be made, leading to important physical insight into the core-guided modes and their differential loss. In particular, we find that when the gaps between the tubes are small, loss is dominated by coupling to the modes confined within the tubes, Fig. 1(e), as they are the largest of the cavities in the cladding (this is less true for nested and multiply nested geometries). The loss of cladding tube modes is significantly higher than those guided in the core due to the proximity of the jacket glass and the smaller radius of the tubes compared to the core. For example, using the models of [20], for a tube of radius 19.5 μm, thickness 530 μm at wavelength 1550 μm, the loss is 52000 dB km^{-1}. Because the field distributions within such cylindrical tube waveguides and their propagation constants can be calculated analytically, this makes the analysis of the coupling process more tractable.

In the following section, we examine the relationship between these cladding tube modes and the loss of the core-guided modes from a coupled-mode perspective. We start by showing detailed numerical simulations justifying our restriction to the analysis of tube modes and then compare calculated loss to quantitative predictions from this analysis.

3. Loss through coupling to tube modes

Great insight into the loss of ARF can be obtained by analyzing the Poynting flux in the radial direction at the perimeter of the fibre which indicates the local leakage loss from the structure. This azimuthally resolved radial Poynting flux, together with transverse power flow analysis is a powerful tool that can link leakage loss to specific geometric features. For example, its use has led to the design of new fibre geometries with ultra-low leakage loss [21]. Here, we apply such analysis to a tubular fibre, to reveal which cladding *modes* the light is coupled into as it leaves the core and show the results in Fig. 2. Using a commercial finite element solver (COMSOL Multiphysics v5.5), we first solved for the modes of a large-core ARF ($R = 32\lambda_0$), having 12 cladding tubes of radius $r = 0.26R$, thickness $t = 530\,\mu m$ and gap size $d = 5.8\,\mu m$. A structure with 12 tubes was chosen that will guide many core modes with low loss [8]. The wavelength of operation was chosen at $\lambda_0 = 1550\,\mu m$. We define the normalized frequency as [22]:

$$F = \frac{2t}{\lambda}\sqrt{n_{\text{glass}}^2 - n_{\text{a}}^2} \tag{3}$$

with n_{glass} the refractive index of the dielectric tubes and n_{a} the refractive index of the air regions. The operating wavelength, λ_0 corresponds to a normalized frequency, $F = 0.71$ and is located at the minimum loss of the fundamental anti-resonant window (see Fig. 1(b)). At this wavelength, no mode confined in the thin silica membranes, Fig. 1(g), interacts appreciably with the core modes [23], suggesting that leakage via modes located in air alone should be able to account for the loss.

In Fig. 2(a–d) we overlay the azimuthally-resolved loss with the geometry of the fibre. It can be seen that leakage loss peaks at the azimuthal locations of the tubes, indeed more than 90% of leakage loss occurs within ±5° of the centre of the tubes. This is indicative of the fact that the loss is caused by the coupling to the cladding tube modes. We observe that the magnitude of the peaks is different, depending on the azimuthal position of the cladding tube, eg. in Fig. 2(a) the peaks are minimum at 30° and 210° and maximum at 150° and 330°. This be attributed to the electric field polarisation; leakage loss is higher where the transverse electric field is normal to the jacket as expected when considering the difference in reflection coefficient, described by Fresnel's equations, for *s* and *p* polarizations.

To confirm that coupling to tube modes is the origin of loss, we examine the extent to which core modes are hybridised with cladding modes. For each core mode we measure the fraction of modal power, given as the time averaged Poynting vector in the direction of propagation, located and propagating inside the cladding tube. Fig. 2(e) compares, for the fundamental HE_{11} mode, the power inside each tube to the azimuthally-resolved power flux. For all tubes, the relative magnitude of the tube power almost exactly matches that of the corresponding peak in the power flux. This is the case for all of the core modes considered (eg. Figs. 2(f-h)). Considering other modes we observe that the fraction of power in tubes increases with the mode order as does the total amount of leakage through the tubes; the maximum and minimum powers for the fundamental HE_{11} mode (Fig. 2(e)) are 2 orders of magnitude lower than the EH_{12} (Fig. 2(h)) mode. Given the strong association of loss to the degree of coupling it is logical to say that the primary source of loss is via the tubes. This is an indication that confinement loss can be directly linked to coupling to tube modes and that a tube coupling model can be used for quantitative prediction of the modal loss.

As further evidence, we show in Fig. 3 the correlation, for 40 core-guided modes, between the confinement loss and total fraction of power in the cladding tubes. The fraction of power in the cladding (Region B) increases with mode order as expected for less confined modes. However this is not proportional to the increase in confinement loss. The fraction of power in the tubes (Region A) on the other hand shows excellent correlation with confinement loss, supporting our claim that the loss of all core-guided modes in tubular anti-resonant fibre is primarily due to coupling to tube modes.

It is also interesting to note that for the relatively low-loss lower-

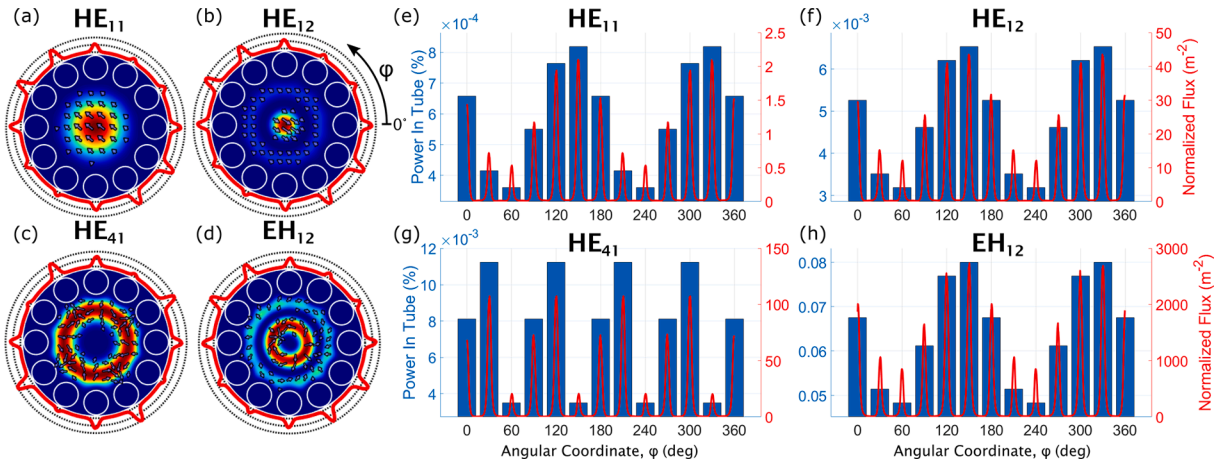

Fig. 2. (a–d) Mode plots of several core modes that have been numerically simulated, black arrows superimposed on the mode denote the transverse electric field vectors. Around the perimeter of each mode figure we plot the radial power flux (red line), normalized to the total modal power, as a function of the angular coordinate ϕ. (e–h) The percentage of the total modal power flow in the axial direction inside individual cladding tubes (blue bars) superimposed with the normalized radial flux. In order to emphasize the relationship between the two quantities we have repeated the bar for the tube at 0°/360°.

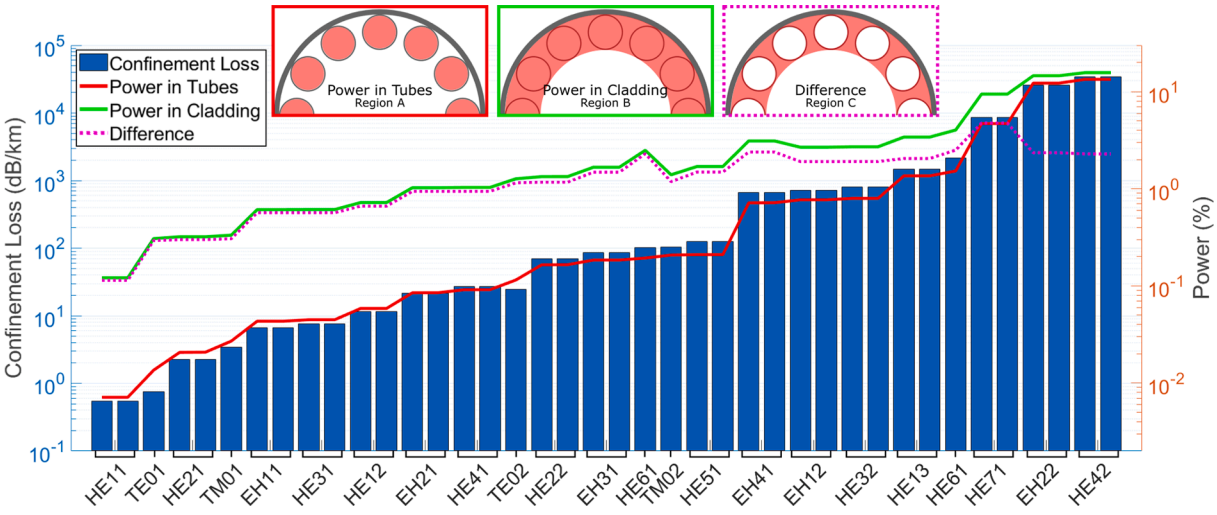

Fig. 3. The confinement loss of the core modes of a large core tubular ARF (blue bars) and the percentage of the total modal power propagating in various regions of the cladding (lines), the regions A, B and C are highlighted in red in the insets.

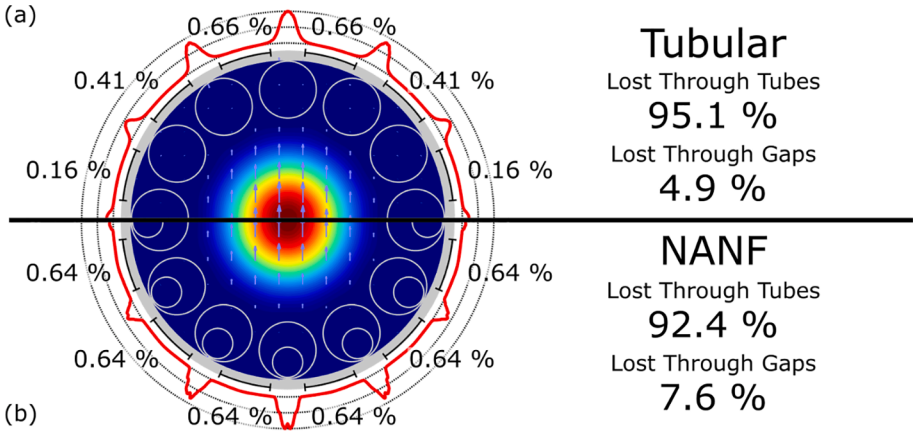

Fig. 4. The normalized radial power flux at the jacket of the fundamental mode in (a) tubular and (b) NANF fibre. The black arcs centred on the gaps show a 12° angle. The loss through this angle is calculated and displayed as a percentage of the total loss.

order, core-guided modes, most of the power outside of the core is propagating *outside* the tubes (in Region C). For the HE_{11} modes in this fibre, 0.12% of the total power propagates outside the core (in Region B) however, only 5.9% of that power resides inside the cladding tubes (Region A). As the loss increases a higher fraction of the cladding power is found to reside inside the tubes: for the HE_{22} mode 1.3% of the power propagates in the cladding of which 12.4% propagates in the tubes. Modes very near phase matching are strongly hybridised with cladding modes and the tubes are found to contain more power than the rest of the cladding: the EH_{22} mode has 83.9% of power in the cladding propagating in the tubes and for the HE_{42} mode this figure is 85.4%.

Air modes that are guided in the gap regions between the tubes account for some of the extra power in the cladding. From all we have shown above, it is logical to expect that these gap modes contribute significantly to loss in tubular anti-resonant fibres when the gap between the tubes is large as confirmed by the study in ref [24]. For lower loss geometries with smaller gaps, for example as defined in this work $d < 4\lambda$, these gap-modes have a much smaller impact compared to the tube modes. To compare this behaviour to designs with reduced leakage through tubes we compare the 12-tube fibre of Fig. 1(a) with a NANF that is identical with the exception of the addition of a nested tube. In Fig. 4(a) we examine the fraction of the power lost through the tubes compared to through the gaps. In the case of the tubular fibre, less than 5% of the total leakage is through the gaps. For the NANF in Fig. 4(b) the nested tube reduces the size of the cladding tube air regions and therefore increases the phase-mismatch between the core and cladding tube modes. According to (1) this reduces the loss due to coupling to the tube modes and we therefore observe instead a slightly higher proportion of the total loss associated with the gaps, 7.4%. The exact value depends on the size of the nested element, with lower loss geometries having a higher proportion of that loss through the gaps. Although this study focuses on tubular fibre we believe that the insights gained herein remain applicable to more complex ARFs with nested elements such as the NANF.

4. Quantifying coupling to tube modes

Having shown that the primary source of confinement loss in low-loss tubular fibre is via coupling to the modes of the cladding tubes, we investigated the coupling process between core-guided modes and said tube modes. From Eqs. (1) and (2), the loss of a given core mode scales with the strength of its coupling to the tube modes and inversely with how well it is phase matched to such modes. The latter has provided a direct route to engineering for example effectively single mode guidance in ARFs [25,8].

In this further investigation, we seek to study how the loss of any core mode depends on the separation between its propagation constant and that of cladding tube modes. This required us to simulate a range of ARFs for which the propagation constant of the core and cladding modes can be controlled. In [20], an analytical formula for propagation constants of HE modes confined inside a dielectric tube waveguide was presented as:

$$\beta_{nm} = \frac{k_0(n_{\text{glass}}^2+1)}{2}\left\{ n_a - \frac{1}{2}\frac{u_{nm}^2}{k_0^2 n_a r^2} - \frac{u_{nm}^2}{k_0^3 n_a^2 r^3}\frac{\cot(k_0 t\sqrt{n_{\text{glass}}^2-n_a^2})}{\sqrt{n_{\text{glass}}^2-1}}\right\} \tag{4}$$

with k_0 the free space wavenumber, r the tube radius, and u_{nm} characterises a mode of azimuthal order n and radial order m and satisfies $J_{n-1}(u_{nm}) = 0, J_{n-1}(x)$ being the Bessel function of the first kind [20]. It follows therefore that the propagation constant of the cladding tube modes can be modified either through changing the size of the tubes, or by changing the medium with which they are filled. Changing the tube size to increase or decrease the effective index of the tube modes would result in either changing the number of tubes or the size of the gaps between them and the proximity of the jacket glass. Such changes to the geometry are known to impact the loss of the core modes on their own. Instead, in our simulations we chose to modify the refractive index of the hollow regions inside the cladding tubes, n_a, whilst keeping that of the core and of the glass constant and with no changes to the overall geometry. The magnitude of the change in refractive index we examine is less than 0.1% the contrast of air and glass and so has a negligible impact on the anti-resonance conditions.

Fig. 5 shows the results of our study in which we have taken the geometry of Fig. 1a) and modified the refractive index of the material within the cladding capillaries between 0.9999 and 1.0005 in order to manipulate the propagation constant of the cladding tube modes. A change in refractive index from 0.9999 to 1 corresponds to geometric change in radius of less than 1.5 μm for the geometry considered here (see (4)). Acquiring solutions for core modes with propagation constant lower than that of the HE_{21} cladding tube mode proved to be computationally expensive and time consuming, so we limit our study to modes above it, without loss of generality. In Fig. 5(a) we confirm that the propagation constants of the core modes (solid horizontal lines) are effectively constant, whilst those of the cladding modes (dashed lines) vary approximately linearly with the refractive index. We plot the propagation constant relative to that of the fundamental mode to make clearer the relationship with $\Delta\beta$. Where the propagation constant of the core modes and fundamental cladding tube mode intersect, the phase match condition, $\Delta\beta \approx 0$ is satisfied and strong coupling occurs according to (1). Core modes belonging to the same LP mode group are typically approximately degenerate, their phase constants are nearly equal. We therefore simplify our discussion by referring to modes using their LP group name from this point onward. When calculating cladding tube modes we take the phase constant and loss of the group to be that of the HE mode belonging to that group.

In Fig. 5(b) the confinement loss of the first 4 core mode groups is plotted and we highlight the point of phase matching. For each mode the loss increases as phase matching is approached. Very near to phase matching we find that, owing to the strong hybridisation between core and cladding modes, it is very difficult to label the solutions of the numerical solver as specific core modes and so they are not included in this graphic. This results in the gaps noticeable near phase matching.

Further insight can be gained by plotting the confinement loss of all core modes versus the difference in propagation constant between the core and fundamental cladding tube mode, Fig. 5(c). Here, we have introduced the notation: $\Delta\beta_q = \beta_{\text{core}} - \beta_q$ having the meaning of the difference in propagation constant between a core mode and the specified cladding tube mode group, q. Hence, phase matching with the fundamental, LP_{01}, cladding tube modes occurs at $\Delta\beta_{\text{LP01}} = 0$. The difference in phase constant between cladding modes remains approximately constant (see (4)) so phase matching to the second cladding mode, HE_{21}, occurs at $\Delta\beta_{\text{LP01}} = -2800m^{-1}$. Very near phase matching, $\Delta\beta \approx 0$, the strong coupling between core and cladding tube modes means that the loss suffered by the core mode is very similar to that of an isolated tube mode. The loss of such modes can be estimated with analytical expressions by Zeisberger et al. or Bird [20,26]. Taking the tubes to be an $N = 1$ geometry (as [26]) we have calculated the loss. In Fig. 5(c) we find that this analytically calculated loss well describes the asymptotic peak value of the core modes at phase matching.

Looking at the plots of Fig. 5(c), we can see clearly the Lorentzian-like behaviour of the loss as a function of $\Delta\beta$ as may be expected from (1). Indeed, at phase matching, all the core modes experience high loss as a result of the resonant out-coupling to tube modes. As $|\Delta\beta|$ increases, the loss falls off sharply towards a minimum value. This results in a series of low-loss "windows" between the phase matching points, conceptually similar to anti-resonant windows in wavelength that occur between the resonant modes in the glass membranes [15].

For all the modes, we see that the lowest loss is achieved in the first window, i.e., $\Delta\beta_{\text{LP01}} > 0$ on the figure. Looking at Fig. 5(c), the minimum loss in the second window is nearly two orders higher than the lowest loss achievable in the first. This can be explained by considering

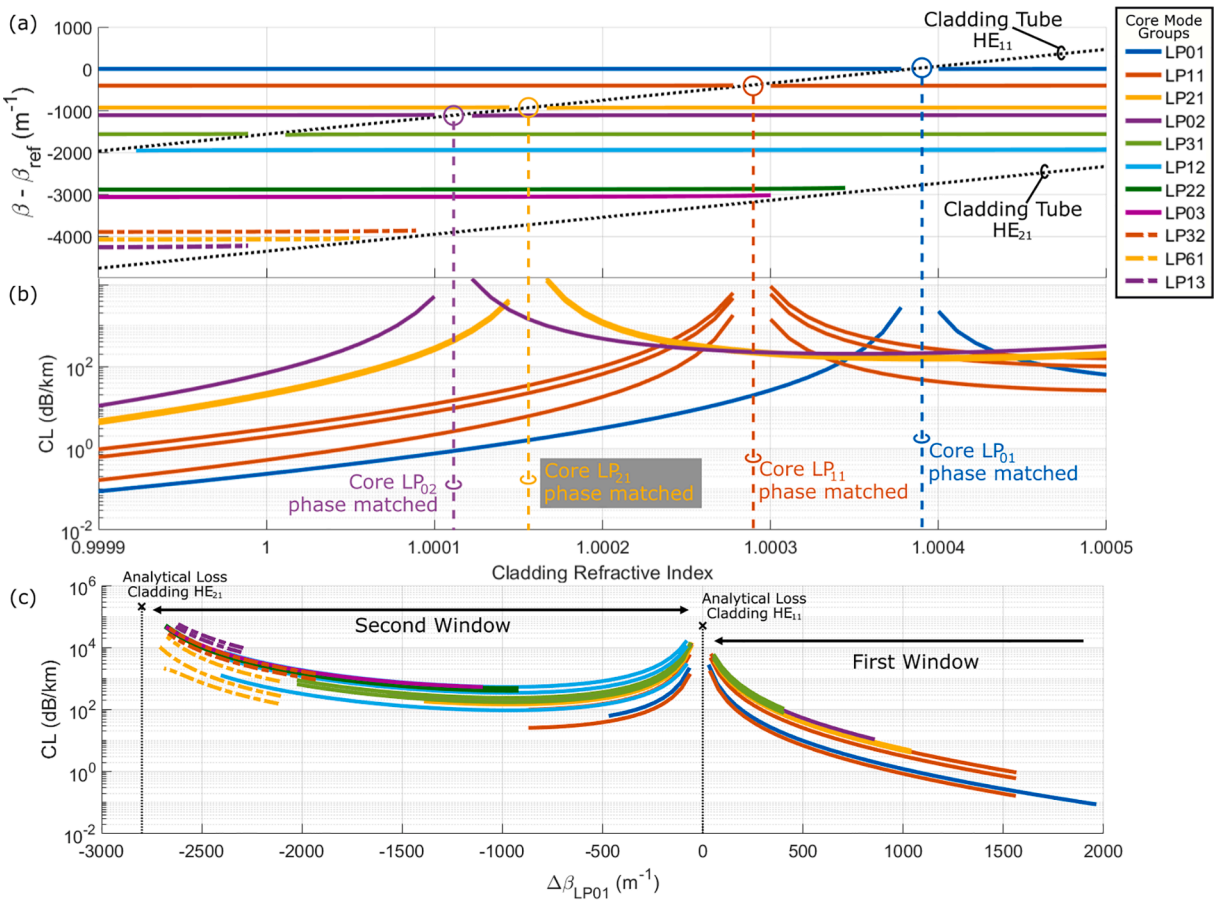

Fig. 5. Numerical simulation of the tubular fibre (Fig. 1(a)) for which we control the refractive index of the air within the cladding tubes. (a) The propagation constant of the core and cladding modes relative to β_{ref} which we take as the propagation constant of the fundamental, LP_{01}, core mode. The propagation constant of the cladding modes is calculated using (4). (b) The confinement loss of the first 4 core modes. The x-axis of (a) and (b) are shared; the vertical dashed lines highlight the points at which the propagation constant of the first 4 core modes intersects with that of the fundamental cladding tube mode. (c) The confinement loss of all the core modes plotted against their difference in propagation constant to the fundamental cladding modes. The black crosses indicate the predicted loss of the first two cladding modes using the model of Bird [26].

that in the second window not only the HE_{11} tube mode will contribute but also the lossier HE_{21} mode. This observation has practical significance when designing ARFs with specific modal properties. If for example multimode guidance is desired with relatively low differential loss between the modes, then all such modes should preferably be guided in the first window, $\Delta\beta_{\mathrm{LP01}} > 0$. Conversely, when aiming to outcouple a specific mode, for example to achieve effectively single mode guidance, it can be more desirable to target a geometry that guides that core mode just inside the second window rather than exactly at phase matching. For small, negative $\Delta\beta_{\mathrm{LP01}}$ loss remains high and the fibre will be more robust against variations in fabrication or bending that would alter the propagation constants of core and cladding modes.

To further interrogate this coupling behaviour, we examine the magnitude of the amplitude coupling coefficient, κ of (1). For two modes, p and q, described by their normalized electric fields, $\widehat{E}_p$ and $\widehat{E}_q$, we will for simplicity consider the overlap integral [24]

$$\eta_{\mathrm{p,q}} = \iint \widehat{E}_p . \widehat{E}_q^{*} \, dA \tag{5}$$

that is proportional to the coupling coefficient, κ. In coupled mode theory where we would effectively regard the fiber as a directional coupler made of the core and the lossy cladding tubes, we ought to rigorously consider the modes of these different structures when they are isolated and uncoupled. In our case however, an approximation is needed because the core cannot be defined as isolated waveguide. With the knowledge of this difficulty, we approximate the core modes as those guided within the core when surrounded by the cladding tube and which we obtain by finite element simulations. A similar approach to the approximation we use here has been used by Deng et. al. [24]. We can compute the electric fields of the cladding tube air modes analytically by treating them as isolated tubes, an approach previously employed in analysing the dielectric modes of the cladding tubes [15,16]. In this work therefore, overlap integrals are calculated between core modes, numerical solutions of the full fibre, and modes of isolated cladding tubes.

There are a large number of tube air modes as each tube supports its own full set of modes, however, since all the tubes in an ideal fibre are identical, all tube modes belonging to the same mode group have equal propagation constants. We therefore define a overlap integral between a core mode p and a cladding tube mode group Q as $|\eta_{\mathrm{Q}}|^2 = \sum_q |\eta_{p,q}|^2$ where the sum extends over all tubes and all modes belonging to group Q.

In Fig. 6 we calculate, for several of the numerically solved core modes of Fig. 5, the overlap integral between an analytically calculated cladding tube mode and plot against the difference in propagation constant of that tube mode. In Fig. 6(a) we observe that the coefficient of coupling to the fundamental cladding tube mode, η_{LP01}, also exhibits a Lorentzian-like behaviour centred at $\Delta\beta = 0$ where each core mode has a maximum value of η that falls off sharply as $|\Delta\beta|$ increases. This can be understood by considering that core modes become strongly hybridised with cladding modes near phase matching and therefore the electric

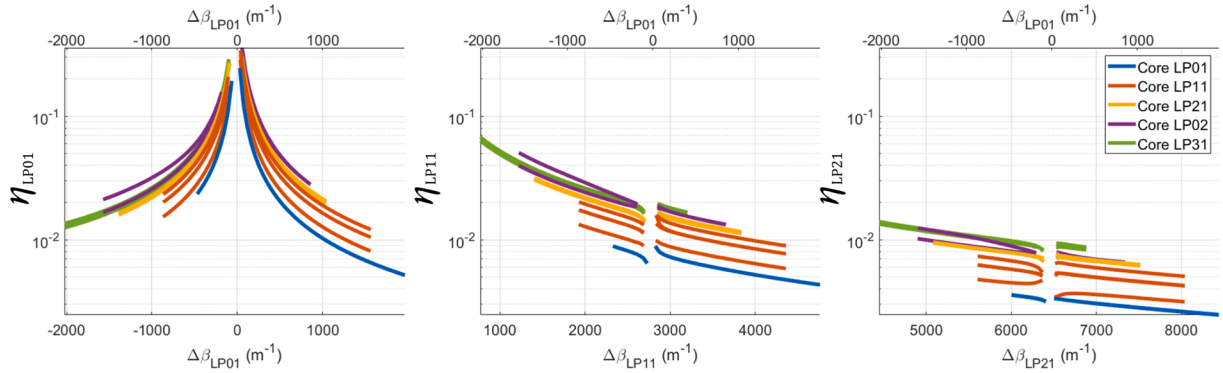

Fig. 6. The overlap integral, (5), between several core modes (line colour) and (a) the LP_{01} cladding tube mode, (b) the LP_{11} cladding tube mode and (c) the LP_{21} cladding tube mode. We plot against the difference in propagation constant between the given core mode and the specified cladding tube mode. The same top x-axis is repeated for (a–c) to emphasize that they share the same range of data.

field overlap with a pure tube mode increases as described by (5).

For the range of data considered, the core modes plotted here are far from phase matching to higher order cladding tube modes (see Fig. 5 (a)). When we calculate the overlap integral to these tube modes in Fig. 6 (b,c), therefore, $|\Delta\beta|$ is large and we observe the tails of a Lorentzian curve.

We find that for all tube modes the magnitude of the overlap integral increases with the core mode order. In Fig. 6(b), the overlap integral of the LP_{11} core mode is almost an order or magnitude larger than of the fundamental LP_{01} core mode. Considering (1), this result goes some way to explain the large differential loss between core modes even when both are in the low-loss first window (see Fig. 5(c)).

Seeking to quantify the loss of the core modes, we find, as in [16], that the loss of core modes can be well approximated by a modified version of (2), that is:

$$\alpha_m^{core} \approx \sum_k \frac{\gamma_k |\eta_{m,k}(\Delta\beta_{m,k})|^2}{\delta^2 + (\Delta\beta_{m,k})^2} \tag{6}$$

where we have introduced the δ to account for the finite loss when $\Delta\beta = 0$ and have made explicit the dependence of the coupling strength on $\Delta\beta$.

Fitting (6) to the simulation data, we do indeed find good agreement. In Fig. 7 we compare the predicted loss from this simple coupling model with the results of numerical simulations for two core modes. These low order core modes are near the phase matching condition with the fundamental cladding tube mode, indeed the point of phase matching ($\Delta\beta_{LP01} = 0$) is contained in this data set. We clearly see that this cladding mode is the most significant contributor to the loss; when considering only the fundamental cladding tube mode in Figs. 7(a,d) there is already some agreement to the data.

When including the contributions of all three cladding tube modes

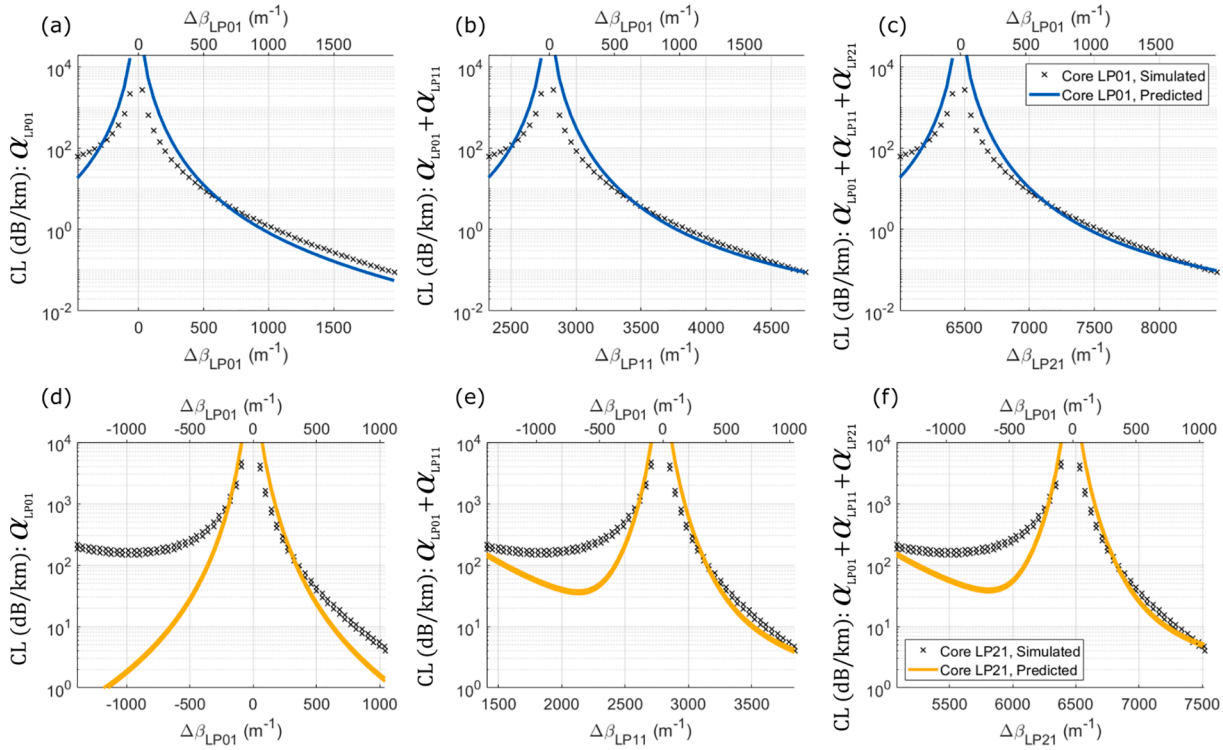

Fig. 7. The confinement loss for (a,b,c) the LP_{01} core mode and (d,e,f) the LP_{21} core mode found by fitting (6) to the simulation data. We show the contribution of (a, d) the fundamental LP_{01} cladding tube mode, (b,e) the LP_{01} and LP_{11} cladding mode groups and (c,f) the LP_{01}, LP_{11} and LP_{21} cladding mode groups. We plot the loss versus the difference in propagation constant between the core mode of interest and the specified cladding tube mode, ie. in (b) $\Delta\beta_{LP11} = \beta_{LP01}^{\text{core}} - \beta_{LP11}^{\text{cladding}}$.

considered here (Figs. 7(c,f)) our model does slightly overestimate the loss very near the phase-matching point which is likely due to the approximations made by the introduction of δ in (6). We also observe a very localised underestimate of loss in the region at the edge of the second window (eg. $\Delta\beta_{LP21} = 5900\,\mathrm{m}^{-1}$ in Fig. 7(f)). In this region, although the fit is improving as additional tube modes are considered, our model appears inadequate to describe the complex interplay between modes. Improvements could be found by considering the phase change of the tube modes in the presence of strong hybridization and due to coupling between individual tube modes.

Eq. 6 describes a summation over all cladding modes but here we calculate only up to the third, LP_{21}, cladding tube mode. As we include the contributions of additional cladding tube modes we observe that the fit improves. To truly capture the loss using this model it would be required to calculate the phase mismatch and overlap with all of the cladding modes including the dielectric modes and the air modes of the inter-tube regions. We do find, however, that very reasonable agreement is found using 3 or even only 2 cladding tube modes in the first window ($\Delta\beta_{LP01} > 0$) that is where we typically desire low-loss modes to be guided.

Here we have explored the powerful concept of mode-coupling for understanding and analysing the behaviour of anti-resonant fibres in the regimes in which they are typically operated. Although the concept of modifying material index we explored here can be studied in practice by modifying for example the gas pressure inside the tubes [27], in a more typical deployment, controlling the phase matching condition must be achieved by controlling the difference in size between the core and cladding tubes. Without adding additional tubes, smaller tubes have wider gaps and larger air regions between them. The gap modes therefore become more significant and, in addition to the effect of coupling to tube modes one must also consider the effect of coupling to gap modes even for low-loss structures where gap modes have a lesser effect. The effect of gap modes in NANFs is increased by virtue of loss to cladding tube modes being reduced and so gap modes are expected to be more important to the analysis of NANFs.

The results shown here could be applied to a number of practical applications, for instance in designing multi-mode ARFs. Previous work has shown how the size of the core impacts the number of low-loss modes guided [11] but these studies ignored the effect of resonant out-coupling when in fact this is currently the primary method of engineering the modes of ARFs. Here, we have shown that the first window is the only regime in which low-loss guidance can be achieved and that phase matching to the fundamental cladding tube mode well describes the loss of the fundamental and higher order core modes in this region. We believe that this knowledge can guide the development of a technique for designing ARF geometries which guide a desired number of modes under a loss threshold.

5. Conclusion

We have shown that in low-loss, anti-resonant fibers with non-contacting cladding tubes, the confinement loss for core-guided modes operating in low-loss regions can be analysed and understood as the result of coupling to cladding tube modes. Air guided modes propagating in the gaps between tubes and dielectric modes in the tubes themselves on the other hand have very little impact on the loss in low-loss regions. A crucial quantity that drives the strength of coupling to tube modes and thus loss, is the separation between the propagation constants of the core and cladding tube modes. When exactly phase matched, core modes suffer losses as high as that of the cladding modes themselves. From the results here we have derived some useful insight into the design of few-moded, multi-moded and effectively single moded ARF. All desired modes must be guided with propagation constant greater than that of the cladding tube modes to achieve low loss for all of them. In tubular fibre this might require choice of small cladding tubes which can cause high loss due to the jacket glass being closer to the core, however, geometries with nested elements such as NANFs can guide multiple low-loss modes without prohibitively high losses [8].

Using our intuitive understanding we were able to develop a model based on resonant coupling to tube modes which, by considering only the contributions of the first three cladding tube modes, showed good agreement to numerical simulation. This model demonstrates that the loss of core modes is dependant on not just coupling to the fundamental cladding tube mode but also to the higher-order cladding tube modes.

CRediT authorship contribution statement

William Shere: Conceptualization, Methodology, Investigation, Writing - original draft. **Gregory T. Jasion:** Conceptualization, Methodology, Writing - review & editing. **Eric Numkam Fokoua:** Conceptualization, Methodology, Writing - review & editing. **Francesco Poletti:** Conceptualization, Writing - review & editing, Supervision.

Declaration of Competing Interest

The authors declare that they have no known competing financial interests or personal relationships that could have appeared to influence the work reported in this paper.

References

[1] M. Michieletto, J.K. Lyngsø C. Jakobsen, J. Lægsgaard, O. Bang, T.T. Alkeskjold, Hollow-core fibers for high power pulse delivery, Optics Express 24(7) (2016) 7103–7119. doi:10.1364/OE.24.007103. url: http://www.opticsexpress.org/abstract.cfm?URI=oe-24-7-7103.

[2] F. Benabid, F. Couny, J.C. Knight, T.A. Birks, P.S.J. Russell, Compact, stable and efficient all-fibre gas cells using hollow-core photonic crystal fibres, Nature 434 (7032) (2005) 488–491, https://doi.org/10.1038/nature03349.

[3] G.T. Jasion, T.D. Bradley, K. Harrington, H. Sakr, Y. Chen, E.N. Fokoua, I.A. Davidson, A. Taranta, J.R. Hayes, D.J. Richardson, F. Poletti, Hollow Core NANF with 0.28 dB/km Attenuation in the C and L Bands, in: Optical Fiber Communication Conference Postdeadline Papers 2020, Optical Society of America, San Diego, California, 2020, p. Th4B.4. doi:10.1364/OFC.2020.Th4B.4. url: http://www.osapublishing.org/abstract.cfm?URI=OFC-2020-Th4B.4.

[4] H. Sakr, Y. Chen, G.T. Jasion, T.D. Bradley, J.R. Hayes, H.C.H. Mulvad, I. A. Davidson, E. Numkam Fokoua, F. Poletti, Hollow core optical fibres with comparable attenuation to silica fibres between 600 and 1100 nm, Nat. Commun. 11 (1) (2020) 6030, https://doi.org/10.1038/s41467-020-19910-7.

[5] H. Sakr, T.D. Bradley, G.T. Jasion, E.N. Fokoua, S.R. Sandoghchi, I.A. Davidson, A. Taranta, G. Guerra, W. Shere, Y. Chen, J.R. Hayes, D.J. Richardson, F. Poletti, Hollow Core NANFs with Five Nested Tubes and Record Low Loss at 850, 1060, 1300 and 1625nm, in, Optical Fiber Communications Conference and Exhibition (OFC) 2021 (2021) 1–3.

[6] E.A.J. Marcatili, R.A. Schmeltzer, Hollow metallic and dielectric waveguides for long distance optical transmission and lasers, Bell Syst. Technical J. 43 (4) (1964) 1783–1809.

[7] P. Uebel, M.C. Günendi, M.H. Frosz, G. Ahmed, N.N. Edavalath, J.-M. Ménard, P. S. Russell, Broadband robustly single-mode hollow-core PCF by resonant filtering of higher-order modes, Opt. Lett. 41 (9) (2016) 1961–1964, https://doi.org/10.1364/OL.41.001961, url: http://ol.osa.org/abstract.cfm?URI=ol-41-9-1961.

[8] W. Shere, G.T. Jasion, E.N. Fokoua, F. Poletti, Low Loss, Large Bandwidth Antiresonant Hollow-Core Fiber Design for Short-Reach Links, in: Optical Fiber Communication Conference (OFC) 2020, OSA Technical Digest, Optical Society of America, San Diego, California, 2020, p. W4D.3. doi:10.1364/OFC.2020.W4D.3. url: http://www.osapublishing.org/abstract.cfm?URI=OFC-2020-W4D.3.

[9] R. Safaei, G. Fan, O. Kwon, K. Légaré, P. Lassonde, B.E. Schmidt, H. Ibrahim, F. Légaré, High-energy multidimensional solitary states in hollow-core fibres, Nature Photon. 14 (12) (2020) 733–739, https://doi.org/10.1038/s41566-020-00699-2.

[10] F. Poletti, Nested antiresonant nodeless hollow core fiber, Optics Exp. 22 (20) (2014) 23807, https://doi.org/10.1364/OE.22.023807, url: https://www.osapublishing.org/oe/abstract.cfm?uri=oe-22-20-23807.

[11] B. Winter, T.A. Birks, W.J. Wadsworth, Multimode Hollow-Core Anti-Resonant Optical Fibres, in: Frontiers in Optics + Laser Science APS/DLS, The Optical Society, Optical Society of America, Washington, DC, 2019, p. JTu4A.18. url: http://www.osapublishing.org/abstract.cfm?URI=LS-2019-JTu4A.18.

[12] P. Zhao, Y. Zhao, H. Bao, H.L. Ho, W. Jin, S. Fan, S. Gao, Y. Wang, P. Wang, Mode-phase-difference photothermal spectroscopy for gas detection with an anti-resonant hollow-core optical fiber, Nat. Commun. 11 (1) (2020) 847, https://doi.org/10.1038/s41467-020-14707-0.

[13] D.C. Allan, N.F. Borrelli, M.T. Gallagher, D. Müller, C.M. Smith, N. Venkataraman, J.A. West, P. Zhang, K.W. Koch, Surface modes and loss in air-core photonic

bandgap fibers, in: Proc.SPIE, vol. 5000, 2003. url: https://doi.org/10.1117/12.480052.

[14] J.A. West, C.M. Smith, N.F. Borrelli, D.C. Allan, K.W. Koch, Surface modes in air-core photonic band-gap fibers, Optics Exp. 12 (8) (2004) 1485–1496, https://doi.org/10.1364/OPEX.12.001485, url: http://www.opticsexpress.org/abstract.cfm?URI=oe-12-8-1485.

[15] L. Vincetti, Empirical formulas for calculating loss in hollow core tube lattice fibers, Optics Exp. 24 (10) (2016) 10313–10325, https://doi.org/10.1364/OE.24.010313, url: http://www.opticsexpress.org/abstract.cfm?URI=oe-24-10-10313.

[16] L. Vincetti, L. Rosa, A simple analytical model for confinement loss estimation in hollow-core Tube Lattice Fibers, Optics Exp. 27 (4) (2019) 5230–5237, https://doi.org/10.1364/OE.27.005230, url: http://www.opticsexpress.org/abstract.cfm?URI=oe-27-4-5230.

[17] Y.Y. Wang, N.V. Wheeler, F. Couny, P.J. Roberts, F. Benabid, Low loss broadband transmission in hypocycloid-core Kagome hollow-core photonic crystal fiber, Opt. Lett. 36 (5) (2011) 669, https://doi.org/10.1364/OL.36.000669, url: https://www.osapublishing.org/DirectPDFAccess/2C3138D4-9841-3FAD-4DCCE61B7850D574_210178/ol-36-5-669.pdf?da=1&id=210178&seq=0&mobile=nohttps://www.osapublishing.org/abstract.cfm?URI=ol-36-5-669.

[18] F. Poletti, J.R. Hayes, D.J. Richardson, Optimising the Performances of Hollow Antiresonant Fibres, in: 37th European Conference and Exposition on Optical Communications, OSA Technical Digest (CD), Optical Society of America, Geneva, 2011, p. Mo.2.LeCervin. 2. doi:10.1364/ECOC.2011.Mo.2.LeCervin.2. url: http://www.osapublishing.org/abstract.cfm?URI=ECOC-2011-Mo.2.LeCervin.2.

[19] F. Yu, W.J. Wadsworth, J.C. Knight, Low loss silica hollow core fibers for 3–4 μm spectral region, Optics Exp. 20 (10) (2012) 11153–11158, https://doi.org/10.1364/OE.20.011153, url: http://www.opticsexpress.org/abstract.cfm?URI=oe-20-10-11153.

[20] M. Zeisberger, M.A. Schmidt, Analytic model for the complex effective index of the leaky modes of tube-type anti-resonant hollow core fibers, Sci. Rep. 7 (1) (2017) 11761, https://doi.org/10.1038/s41598-017-12234-5.

[21] G.T. Jasion, D.J. Richardson, F. Poletti, Novel Antiresonant Hollow Core Fiber Design with Ultralow Leakage Loss Using Transverse Power Flow Analysis, in: Optical Fiber Communication Conference (OFC) 2019, OSA Technical Digest, Optical Society of America, San Diego, California, 2019, p. Th3E.2. doi:10.1364/OFC.2019.Th3E.2. url: http://www.osapublishing.org/abstract.cfm?URI=OFC-2019-Th3E.2.

[22] F. Couny, F. Benabid, P.J. Roberts, P.S. Light, M.G. Raymer, Generation and photonic guidance of multi-octave optical-frequency combs, Science 318 (5853) (2007) 1118–1121.

[23] L. Vincetti, V. Setti, Extra loss due to Fano resonances in inhibited coupling fibers based on a lattice of tubes, Optics Exp. 20 (13) (2012) 14350, https://doi.org/10.1364/OE.20.014350, url: https://www.osapublishing.org/DirectPDFAccess/343C3BEA-98B1-E7C3-C7D9208A7B0577F2_238266/oe-20-13-14350.pdf?da=1&id=238266&seq=0&mobile=nohttps://www.osapublishing.org/oe/abstract.cfm?uri=oe-20-13-14350.

[24] A. Deng, I. Hasan, Y. Wang, W. Chang, Analyzing mode index mismatch and field overlap for light guidance in negative-curvature fibers, Optics Exp. 28 (19) (2020) 27974–27988, https://doi.org/10.1364/OE.400267, url: http://www.opticsexpress.org/abstract.cfm?URI=oe-28-19-27974.

[25] L. Provino, Effect of nested elements on avoided crossing between the higher-order core modes and the air-capillary modes in hollow-core antiresonant optical fibers, Fibers 6 (2) (2018) 42.

[26] D. Bird, Attenuation of model hollow-core, anti-resonant fibres, Optics Exp. 25 (19) (2017) 23215, https://doi.org/10.1364/OE.25.023215, url: https://www.osapublishing.org/abstract.cfm?URI=oe-25-19-23215.

[27] T.W. Kelly, P. Horak, I.A. Davidson, M. Partridge, G.T. Jasion, S. Rikimi, A. Taranta, D.J. Richardson, F. Poletti, N.V. Wheeler, Gas-induced differential refractive index enhanced guidance in hollow-core optical fibers, Optica 8 (6) (2021) 916–920, https://doi.org/10.1364/OPTICA.424224, url: http://www.osapublishing.org/optica/abstract.cfm?URI=optica-8-6-916.